

Finite element modeling of nonlinear dispersive field line resonances: Trapped shear Alfvén waves inside field-aligned density structures

J. Y. Lu,¹ R. Rankin, and R. Marchand

Department of Physics, University of Alberta, Edmonton, Alberta, Canada

V. T. Tikhonchuk

Centre Laser Intenses et Applications, Université Bordeaux 1, France

J. Wanliss

Embry-Riddle Aeronautical University, Bunnell, Florida, USA

Received 12 May 2003; revised 23 July 2003; accepted 13 August 2003; published 14 November 2003.

[1] Using a new two-dimensional nonlinear finite element model, we investigate the interaction of dispersive shear Alfvén wave (SAW) field line resonances (FLRs) and ion acoustic waves in Earth's magnetosphere. We solve the full set of nonlinear reduced MHD equations self-consistently in arbitrary geometries. Initially, a Cartesian box model is used to demonstrate the reliability of our numerical solution in determining the linear and nonlinear evolution of FLRs. Then the full reduced MHD equations with the effects of electron inertia, ion Larmor radius correction, and electron thermal pressure are solved in dipolar and stretched magnetic topologies. We show that time-dependent dispersion and density steepening lead to localization of a highly structured FLR within an ionospheric (equatorial) density cavity (bump). When nonlinear effects are accounted for, we find that FLRs preferentially form in regions of low wave dispersion. Field line stretching and ponderomotive density redistribution lead to a significant reduction in FLR eigenfrequencies, bringing them into the range of observations. Nonlinear effects also cause a rapid acceleration of the timescale over which small perpendicular spatial scales appear. In our model, it is shown that density perturbations can be comparable to the equilibrium background density.

INDEX TERMS: 2740 Magnetospheric Physics: Magnetospheric configuration and dynamics; 2704 Magnetospheric Physics: Auroral phenomena (2407); 2752 Magnetospheric Physics: MHD waves and instabilities; 2736 Magnetospheric Physics: Magnetosphere/ionosphere interactions; 7827 Space Plasma Physics: Kinetic and MHD theory; *KEYWORDS:* shear Alfvén waves, finite element modeling, auroral processes

Citation: Lu, J. Y., R. Rankin, R. Marchand, V. T. Tikhonchuk, and J. Wanliss, Finite element modeling of nonlinear dispersive field line resonances: Trapped shear Alfvén waves inside field-aligned density structures, *J. Geophys. Res.*, 108(A11), 1394, doi:10.1029/2003JA010035, 2003.

1. Introduction

[2] Field line resonances (FLRs) are standing shear Alfvén waves (SAWs) that form on closed geomagnetic field lines in Earth's magnetosphere. A class of FLRs is commonly observed with frequencies in the range of 1–4 mHz in the nightside magnetosphere and auroral ionosphere [e.g., Ruohoniemi *et al.*, 1991; Samson *et al.*, 1991, 1992]. These FLRs are narrow in the direction perpendicular to the magnetic field, typically on the order of a few tens of kilometers in the auroral ionosphere and up to an R_e or so when mapped

to the equatorial plane (EP). For a highly conducting ionosphere, FLRs have approximate electric and velocity field nodes at the ionosphere and antinodes in the equatorial plane. The perpendicular electric and azimuthal magnetic fields suffer a 180° latitudinal phase shift that is useful in identifying FLRs in observations. Field-aligned currents in FLRs can be on the order of tens of $\mu\text{A}/\text{m}^2$ above the auroral ionosphere [e.g., Walker *et al.*, 1992], whereas azimuthal velocities can be on the order of 1 km/s in the auroral ionosphere but may be as large as 100–200 km/s in the equatorial plane [Walker *et al.*, 1992; Samson *et al.*, 1992].

[3] FLRs are attributed to the coupling of monochromatic compressional waves to SAWs on closed magnetic field lines, at positions satisfying $\omega^2/v_A^2 = k_{\parallel}^2$, where ω is the frequency of the compressional wave driver, v_A is the local Alfvén speed and k_{\parallel} is the wave number along the magnetic

¹Also at Center for Space Science and Applied Research, Chinese Academy of Sciences, Beijing, China.

field [Southwood, 1974; Chen and Hasegawa, 1974]. Possible sources of monochromatic compressional waves include MHD surface waves and/or magnetohydrodynamic (MHD) cavity or waveguide modes that support global MHD compressional waves [Hasegawa, 1976; Samson and Rankin, 1994]. On localized resonant magnetic surfaces, compressional waves convert part of their energy to guided SAWs that form standing waves between the polar ionospheres [Cummings *et al.*, 1969; Cheng *et al.*, 1993; Leonovich and Mazur, 1997]. Provided ionospheric conductivities are high (a few mho), FLRs will grow and narrow [Rankin *et al.*, 1993] due to phase mixing between the driver and excited FLR wave fields. Large-amplitude FLRs and/or FLRs excited in cold plasma can also exert ponderomotive forces (PFs) that drive density depressions in the ambient plasma [Boehm *et al.*, 1990; Rankin *et al.*, 1995, 1999], and in particular, density cavities across a variety of scales are a common feature of auroral zone potential structures [e.g., Persoon *et al.*, 1988; Lundin *et al.*, 1994; Stasiewicz *et al.*, 1997].

[4] If FLRs narrow to a point where the radial scale size is of the order of the ion gyroradius or less, kinetic effects become important. When FLRs narrow to a width of several electron inertia lengths (several kilometers near the ionosphere), parallel electric fields may develop and sharp density gradients may result in mode conversion of SAWs to electron inertia waves [e.g., Goertz, 1984; Wei *et al.*, 1994]. Since nonlinear effects, including the ponderomotive force and harmonic generation, stabilize FLR growth through frequency “detuning” and Alfvén velocity profile modification, mode conversion can ultimately cause saturation in the growth [Rankin *et al.*, 1995] of FLRs. Near the ionosphere, FLR field-aligned currents are large, and it has been speculated that the associated parallel electric fields may accelerate electrons to several hundred eV, resulting in the spatial modulation of auroral arcs [Hasegawa, 1976]. Among these processes, nonlinearity and dispersion are important, leading to soliton formation in the thermal dispersion regime of FLRs and parametric decay instability in the inertial regime. Therefore the relative importance of different nonlinear and dispersive processes results in rich behavior in the nonlinear dynamics of SAWs [Frycz *et al.*, 1998].

[5] Observations and theory [e.g., Wei *et al.*, 1994; Samson *et al.*, 1996; Streltsov and Lotko, 1997; Trondsen *et al.*, 1997; Rankin *et al.*, 1999] suggest that ULF, shear Alfvén field line resonances can produce temporally modulated auroral arcs with frequencies in the range of a few mHz. Using a box model, Streltsov and Lotko [1995] presented a three-dimensional (3-D) linearized MHD calculation of dispersive FLRs including electron inertia and finite pressure. This was the first systematic study on consequences of the transition from negative to positive Alfvén wave dispersion that occurs at intermediate altitudes of 4–6 R_e . Based on the reduced MHD equations derived by Kadomtsev and Pogutse [1974], Strauss [1976], and Hasegawa and Wakatani [1983], Frycz *et al.* [1998] suggested a model describing the nonlinear interaction of dispersive shear Alfvén FLRs and ion acoustic waves (IAWs). Using a similar (box) model, Frycz *et al.* [1998] solved a relatively simple set of envelope (slowly varying amplitude) equations and discussed the contributions of

electron inertia and thermal pressure to the linear and nonlinear dynamics of FLRs. To investigate the evolution of dispersive FLRs in a dipole magnetic field, Rankin *et al.* [1999] extended the work of Frycz *et al.* [1998] and examined the interactions of SAWs and IAWs for a specific magnetic shell $L = 8$ under the envelope approximation. They demonstrated that the combination of the PF and dispersive effects can explain a number of observational features associated with the dynamic structure of discrete auroral arcs. In other two-dimensional FLR modeling, Streltsov and Lotko [1999] investigated the effect of plasma anomalous resistivity and reproduced features of FLR data simultaneously measured by the NASA FAST satellite and instruments of the Canadian CANOPUS array of all-sky imagers and magnetometers. Recently, nonlocal conductivity models that include electron kinetic effects have been suggested for low-frequency SAWs [Tikhonchuk and Rankin, 2002; Lysak and Song, 2003]. These models predict enhanced parallel electric wave fields that may be necessary to explain the observed range of auroral electron precipitation energies.

[6] Existing FLR models often cannot be applied to realistic magnetospheric parameters because they are limited by assumptions of weak nonlinearity and separation of the Alfvénic, dispersive, and sonic time scales (the assumption used in envelope models). To overcome this difficulty, we have developed a new simulation code which solves the full set of reduced MHD equations for dispersive FLRs. Our nonperturbative treatment allows us to investigate the complete dynamics of growth and saturation of wave fields and density perturbations under realistic magnetospheric conditions. Nonlinear and dispersive effects have been incorporated into the finite element code first developed by Marchand and Simard [1997] and the effects of electron inertia and thermal dispersion in a dipolar and stretched magnetic field are presented.

2. Reduced MHD Equations

[7] The derivation of the reduced MHD equations describing the interaction of SAWs and IAWs is based on the following assumptions [Frycz *et al.*, 1998]: (1) perturbations are characterized by a perpendicular scale length (L_{\perp}) that is much smaller than the parallel scale length (L_{\parallel}), i.e., $L_{\perp}/L_{\parallel} \ll 1$; (2) the characteristic time for the evolution of the wave is much longer than the ion gyro period, $1/\omega_{ci}t \ll 1$, where ω_{ci} is the ion gyrofrequency; (3) The ion gyroradius ρ_i is small compared with the characteristic perpendicular scale: $(\rho_i/L_{\perp})^2 \ll 1$; and (4) the plasma remains quasi-neutral. Following Frycz *et al.* [1998] and making use of these assumptions, we have rederived the following set of reduced MHD equations for low frequency plasma

$$\begin{aligned} \nabla \cdot \left[\frac{\rho \mu_0}{B_0^2} \left(1 + \frac{3}{4} \rho_i^2 \nabla_{\perp}^2 \right) \frac{d}{dt} \nabla_{\perp} \phi \right] + \nabla \cdot (\mathbf{b} \nabla_{\perp}^2 A) \\ = \nabla_{\perp} \cdot \left(\frac{\mu_0}{B_0} \mathbf{b} \times \nabla_{\perp} P \right), \end{aligned} \quad (1)$$

$$\frac{\partial A}{\partial t} + \mathbf{b} \cdot \nabla \phi = \lambda_e^2 \frac{\partial}{\partial t} \nabla_{\perp}^2 A + \frac{1}{en_e} \mathbf{b} \cdot \nabla P_e, \quad (2)$$

$$\rho \frac{dV_{\parallel}}{dt} = -\mathbf{b} \cdot \nabla P + \frac{\rho}{B_0^2} \nabla_{\perp} A \cdot \frac{d}{dt} \nabla_{\perp} \phi + \frac{1}{B_0} \mathbf{b} \cdot (\nabla_{\perp} A \times \nabla_{\perp} P), \quad (3)$$

$$\frac{1}{\rho} \frac{d\rho}{dt} = \frac{1}{B_0} \frac{\partial}{\partial t} \delta B_{\parallel} - \nabla \cdot (\mathbf{b} V_{\parallel}), \quad (4)$$

where A is the parallel component of the vector potential, ϕ is the scalar electric potential, ρ is the plasma density, B_0 is the unperturbed magnetic field, e is the elementary charge, P is the plasma pressure, P_e is the electron pressure, n_e is the electron number density, \mathbf{b} is the unit vector along the magnetic field, V_{\parallel} is the ion fluid velocity along the magnetic field, and δB_{\parallel} is the compressional perturbation of the magnetic field. Shear Alfvén waves coupling to density, pressure, and finite ion gyroradius effects are accounted for in equation (1), while equation (2) accounts for electron inertia and electron thermal pressure effects. Equations (3) and (4) describe ion acoustic waves. According to Ampere's law, δB_{\parallel} is associated with the plasma pressure

$$\nabla_{\perp} \delta B_{\parallel} = -\frac{\mu_0}{B_0} \nabla_{\perp} P - \frac{\mu_0 \rho}{B_0^2} \mathbf{b} \times \frac{d}{dt} \nabla_{\perp} \phi. \quad (5)$$

It should be noted that our work differs from that of *Frycz et al.* [1998], *Rankin et al.* [1999], and *Streltsov and Lotko* [1999] in that: (1) we treat the full set of reduced MHD equations, as opposed to linearized/envelope equations; (2) we directly solve the full Ohm's law along the magnetic field line (equation (2)), as opposed to its simplified form; (3) equation (2) uses ∇P_e to calculate the parallel component of the polarization electric field as a consequence of gradients in electron pressure; and (4) we do not assume an isothermal electron response but instead use an adiabatic condition. From equations (2) and (3) it follows that for a nonuniform density profile such as the one assumed in some of our calculations, the isothermal assumption would introduce an initial electric field and an initial acceleration of the plasma in the direction parallel to the magnetic field. Thus for consistency we assume that all species respond adiabatically to perturbations. In our calculation, the ratio of specific heats is $\gamma = 5/3$.

3. Numerical Approach

[8] A two-dimensional finite element code TOPO, developed by Marchand [*Marchand and Simard, 1997; Marchand and Shoucri, 2001*], is used to solve equations (1)–(5). TOPO was originally used to solve the equations governing transport of plasma and neutral particles in a tokamak. We chose this approach to model magnetospheric physics because of the ease with which complex magnetic topologies can be investigated. In particular, the use of unstructured grids considerably simplifies mesh generation in relation to stretched magnetic topologies. In TOPO, equations are cast in the general form

$$\sum_{l=1}^N \left(Z_{kl} \frac{\partial U_l}{\partial t} + \nabla \cdot (\mathbf{A}_{kl} U_l) + \nabla \cdot (\mathbf{B}_{kl} \cdot \nabla U_l) + C_{kl} U_l + \mathbf{D}_{kl} \cdot \nabla U_l \right) + S_k = 0, \quad (6)$$

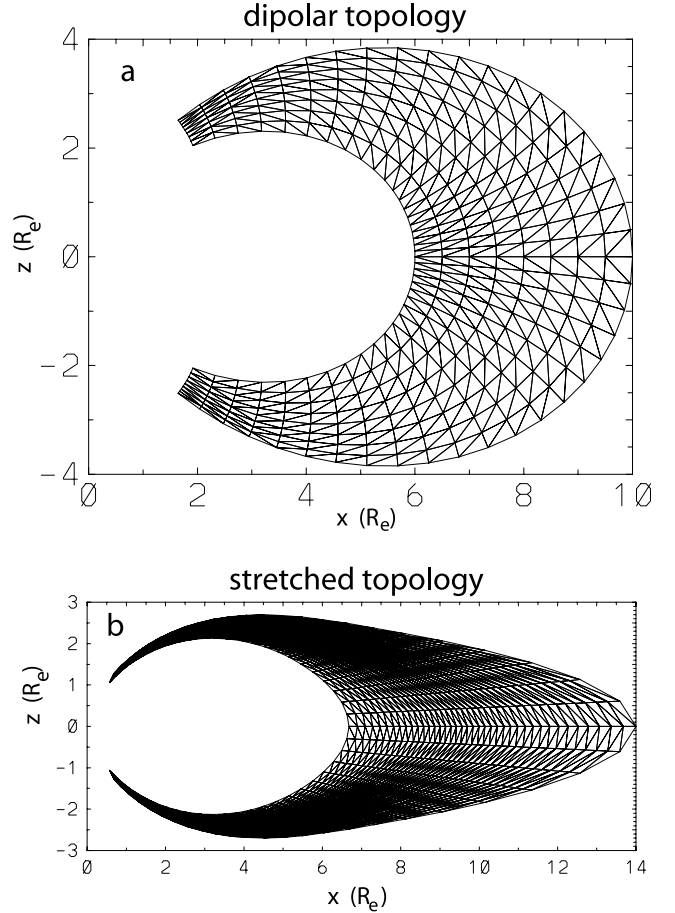


Figure 1. Illustration of unstructured, triangular meshes for (a) a dipolar topology and (b) a stretched topology.

where the indices k and l run from 1 to N for a system of N coupled partial differential equations. In equation (6), U_l is the unknown, Z_{kl} , \mathbf{A}_{kl} , \mathbf{B}_{kl} , C_{kl} , and \mathbf{D}_{kl} are coefficients, and S_k represents a source term for equation k . Any dependence of the coefficients on the unknowns U_l is treated as known (from the previous time step), and all unknowns U_l are otherwise solved fully implicitly. The unknown appearing in the convection term (the term with \mathbf{A}_{kl}) may, however, be treated fully implicitly or semi-implicitly. TOPO allows for a solution by time-splitting the governing equations into a number of groups of equations, each one containing fewer than the total number N of equations. This option is very convenient when solving large systems of equations because it avoids problems associated with the inversion of large sparse matrices. Another advantage of TOPO is that it can solve multi-time-dependent partial differential equations with second-order spatial derivatives. It is therefore capable of incorporating nonlinear and dispersive effects.

[9] In our simulations, a finite element discretization is made between magnetic shells starting at $L = 5$ and ending at $L = 10$ in the dipolar case and $L = 6.5$ – 14 in the stretched field case. We use a triangular and unstructured mesh. Figure 1 gives schematic illustrations of an orthogonal mesh for a dipolar topology and a nonorthogonal mesh for a stretched field topology. In our calculations, depending on the spatial scale of dispersive effects being considered,

much more refined meshes with nonuniform resolution are used. Spurious perpendicular diffusive transport is avoided by aligning the mesh with the magnetic flux surfaces [Marchand and Simard, 1997].

4. FLRs in Box Model MHD

[10] First, we consider a box model magnetosphere with straight magnetic field lines. The main reason for considering this simple magnetic field geometry is that it is an example studied by numerous authors [e.g., Southwood and Kivelson, 1986; Rankin et al., 1993; Streltsov and Lotko, 1995; Frycz et al., 1998; Bhattacharjee et al., 1999]. This case therefore provides a convenient test of our physical model and numerical solution technique. In the box model, x corresponds to the radial coordinate, z is along the field line, and y is in the azimuthal direction. The model parameters are intended to correspond approximately to magnetospheric conditions at the equator: $B = B_z = B_0(1/r)^3$, where $B_0 = 30834$ nT and the plasma density $\rho_0 = 3.345 \times 10^{-23}$ kg/m³. The SAW is driven with an external monochromatic perturbation of the electric potential ϕ . This driving term for ϕ in equation (1) is centered on the shell $L = 7$ at the equator with a Gaussian shape, $Q = Q_0 \sin(\omega t) \exp(-((x - x_0)^2 + z^2)/\Delta^2)$. Here, $x_0 = 7 R_e$, $\Delta = 0.5 R_e$, $Q_0 = 2 \times 10^2$ V/s.

4.1. Linear Box Model FLRs

[11] We first solve the linearized Cartesian form of the equations given in section 2. First, let us recall that the relative importance of different SAW dispersive processes can be estimated from the dispersion parameter [Rankin et al., 1999]

$$\delta = 3\rho_i^2/4 - \lambda_e^2(1 - v_{Te}^2/v_A^2), \quad (7)$$

where v_{Te} and v_A are the electron thermal and Alfvén speeds, respectively. Note that $\delta > 0$ when thermal effects dominate, while $\delta < 0$ when inertial effects dominate. The different signs of δ correspond to different signs of the perpendicular group velocities (inertial waves propagate Earthward while thermal waves propagate anti-Earthward). Beating between the driver and excited waves on adjacent field lines leads to phase mixing and narrowing of the FLR to the inertial or ion-gyro scale. In the linear approximation, dispersive SAWs propagate energy out of the resonant layer at the perpendicular group velocity, leading to linear saturation of the wave field. The linear saturation time and the thickness of the resonant layer at saturation can be estimated from [Rankin and Tikhonchuk, 1998; Frycz et al., 1998]

$$t_s \approx (t_{saw}/2)(l_\omega^2/|\delta|)^{1/3}, \quad l_s \approx (l_\omega|\delta|)^{1/3}, \quad (8)$$

where l_ω denotes the characteristic gradient scale length of the radial variation of the SAW eigenfrequency (determined by the ambient plasma conditions), and t_{saw} is the SAW period. For the simulation parameters described above, linear saturation occurs at about 30 SAW periods and is well approximated by the simple expressions defined above.

[12] Figure 2 shows the structure of an excited dispersive FLR at two instants of time, computed using different values of the dispersion parameter. Specifically, $\delta = -3.47 \times 10^{-5}$

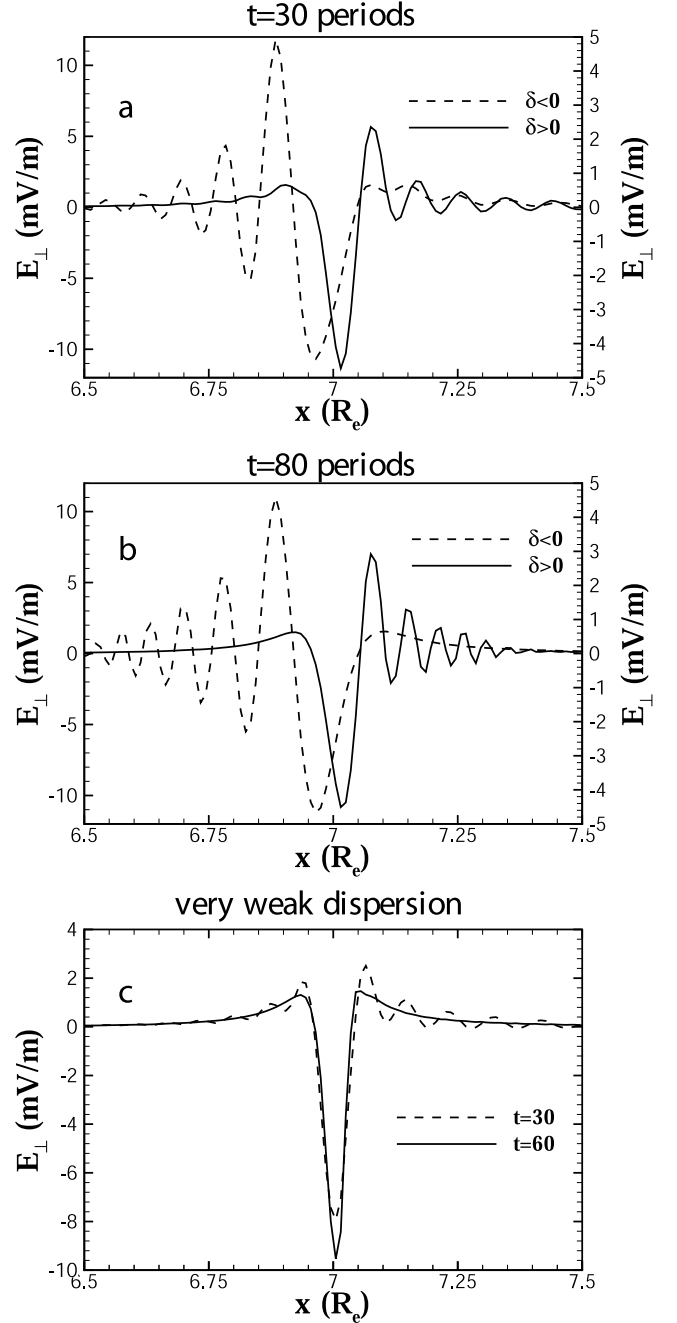


Figure 2. Linear evolution of E_{\perp} for an electron inertia FLR (dashed lines) and a dispersive thermal FLR (solid lines) at $z = 8 R_e$ for (a) $t = 30$ and (b) $t = 80$ in a Box model. Figure 2c shows the linear evolution of a weak dispersive FLR.

R_e^2 (dashed lines) corresponds to excitation of electron inertia dominated FLRs while $\delta = +3.47 \times 10^{-5} R_e^2$ (solid lines) corresponds to excitation of thermally dominated FLRs. The FLR driver is centered on $L = 7$ at $z = 8 R_e$ and results are shown at times corresponding to $t = 30$ (Figure 2a) and $t = 80$ (Figure 2b) SAW periods, respectively. As shown by the dashed lines of Figures 2a and 2b, electron inertia leads to Airy-like solutions with fields propagating Earthward, while in the thermal regime (solid lines), finite ion gyroradius and electron thermal pressure dominate, produc-

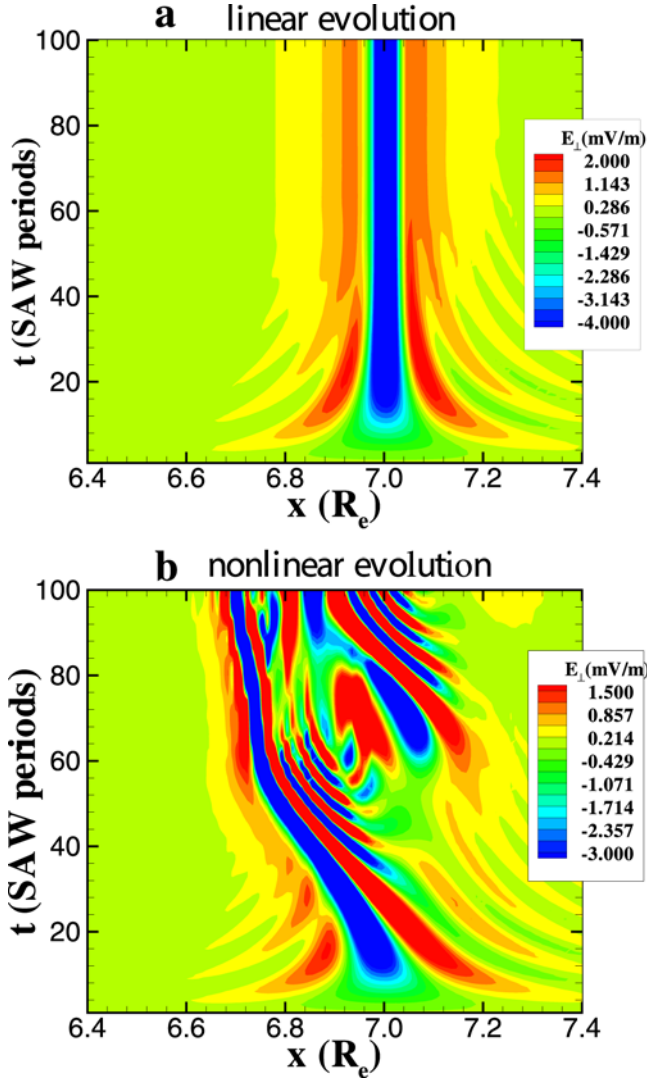


Figure 3. Dynamic evolution of electric field component perpendicular to the magnetic field E_{\perp} at the EP in a Box model: (a) linear case and (b) nonlinear case.

ing anti-Earthward propagating waves. Note that the location of the resonance layer remains unchanged in the linear evolution of dispersive FLRs. Figure 2c shows the FLR linear evolution in the case of very weak dispersion $\delta = +3.0 \times 10^{-6} R_e^2$, at $t = 30$ and 80 periods, respectively. In this case, dispersion is not important in structuring FLRs and in propagating energy away from the resonance layer. Small dispersion mainly acts to stop further narrowing of the resonance layer. Nevertheless, the regime of small dispersion is very important and will be revisited below when we study the nonlinear evolution of FLRs.

4.2. Nonlinear Box Model FLRs

[13] Several new and interesting features are observed in the nonlinear evolution of FLRs. In order to illustrate these effects, the full set of nonlinear equations (1)–(4) is solved again in the box model. To see the effect of nonlinearity, in Figure 3 we compare the linear evolution (Figure 3a) with the nonlinear evolution (Figure 3b) of the weak dispersive electron thermal FLR that was studied above and illustrated

in Figure 2c. Note that in this case, $\delta = +3.47 \times 10^{-6} R_e^2$, corresponding to a warm plasma where thermal pressure and gyroradius effects dominate.

[14] Figures 4a–4b and 4c–4d show the spatial distribution of the SAW field-aligned current and perpendicular electric field at $z = 8 R_e$ and for times $t = 30$ and $t = 80$ periods, respectively. Figures 4d–4e gives the relative density $\delta\rho/\rho_0$ along the field line at $x = 7 R_e$. The dynamic evolution and structure are dramatically different from that observed in the linear case. In the linear case, Figures 2 and 3a, the resonance stays at the driven location and presents itself as a single standing wave structure. However, in the nonlinear case, Figure 3b, the density changes created by the ponderomotive force move the resonance position significantly Earthward, and a much broader and more complicated resonance structure is observed. As shown by the solid lines in Figures 4a and 4c at $t = 30$ periods, anti-Earthward propagating dispersive waves are observed due to the dominance of thermal effects. Later in time, for example at 80 periods, nonlinearity has strongly modified FLR dynamics. A double-peaked ionospheric (equatorial) density cavity (bump) emerges, which acts to trap dispersive Alfvén waves in the inertial (thermal) regime. The formation of ionospheric (equatorial) density cavities (bumps) is an important feature of the nonlinear stage of FLR evolution that will be investigated below in more detail. Figure 4 also demonstrates the effect of the PF in expelling plasma from the ionospheric ends of the field line where density cavities are formed. The expelled plasma moves toward $z = 0$ (the equator) where it accumulates. In Figure 4e, the depth of the density cavities achieves a magnitude of approximately 15% at $t = 30$ periods, while the density accumulation reaches 90% at the EP at $t = 80$ periods (Figure 4d).

[15] The dynamic structure in Figure 3b is quantitatively different from previous work, where either the linearized approach or slowly varying envelope approximation is used [Frycz *et al.*, 1998; Rankin *et al.*, 1999; Streltsov and Lotko, 1999]. In particular, Frycz *et al.* [1998] have shown that nonlinearity (ponderomotive) and electron thermal dispersion can lead to soliton formation in the coupled ion-shear wave evolution of the resonance. This effect is defined by a characteristic parameter that is dependent on the product of the ion-acoustic frequency (assuming a dominant fundamental mode) and a characteristic nonlinear timescale. However, this behavior requires a wide separation of the periods of SAWs and IAWs. In the examples discussed here, this separation of timescales breaks down, and nonlinear effects result in a highly structured and rapidly temporally modulated SAW that becomes trapped inside nonlinear density perturbations. A more detailed discussion is given in section 5.

[16] In the box model the parallel wave current and perpendicular electric field are always too small to explain observations above the auroral ionosphere [e.g., Walker *et al.*, 1992]. A more realistic magnetic topology is discussed in sections 5.

5. Nonlinear Evolution of Dispersive FLRs in Dipolar and Stretched Magnetic Fields

[17] In this section, we apply TOPO in a more realistic geomagnetic topology, namely, that of dipolar and stretched magnetic fields. The dispersion parameter δ no longer has

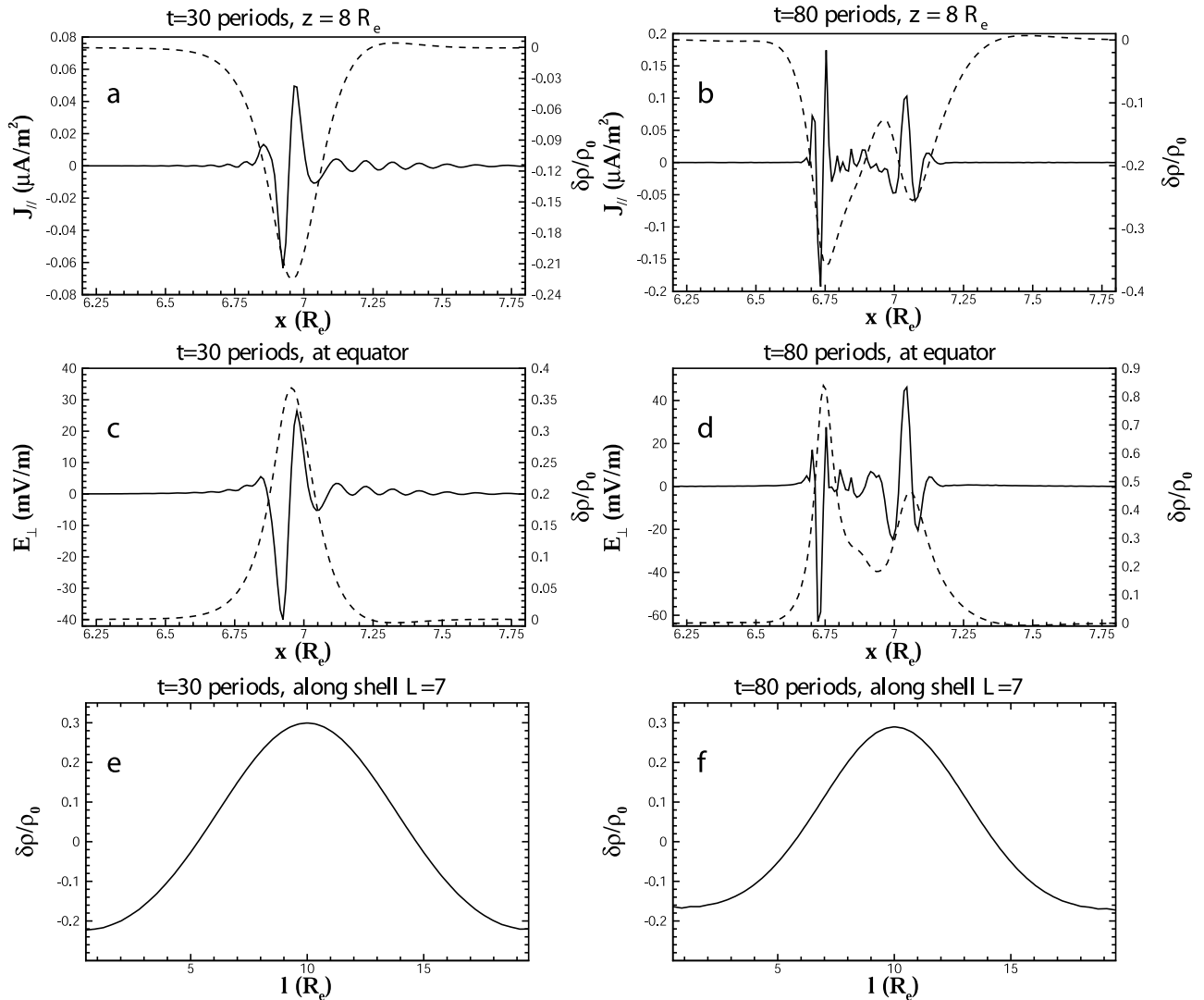


Figure 4. Nonlinear evolution of a dispersive thermal FLR in a Box model: J_{\parallel} at $z = 8 R_e$ for (a) $t = 30$ and (b) $t = 80$ periods; E_{\perp} at the equator for (c) $t = 30$ and (d) $t = 80$ periods; Dashed lines are their corresponding relative densities $\delta\rho/\rho_0$. Figures 3e and 3f are the $\delta\rho/\rho_0$ along the shell $L = 7$ at $t = 30$ and 80 periods, respectively. l corresponds to the distance in Earth radius from the bottom (ionosphere) boundary.

the simple form introduced in the box model. It must now be calculated as a convolution of thermal and inertial contributions along the field line [Rankin *et al.*, 1999]. The wave properties still have the same dependence on the sign of δ , with positive (negative) values indicating the dominance of thermal (inertial) effects on the chosen field line. To proceed, we consider a two-species plasma with a constant density of hydrogen, $n_H = 1 \text{ cm}^{-3}$, and an oxygen component with a density $n_O = 10^2 \text{ cm}^{-3}$ at the ionospheric ends which decreases exponentially with altitude over a scale length $h_O = 600 \text{ km}$: $n_0(s) = n_H + n_O \exp[-(s_{\max} - |s|)/h_O]$, where s is the coordinate along the magnetic field line, with $s = 0$ at the equator. Unperturbed quantities are identified with the subscript zero. Along a given magnetic field line, the initial background electron and ion temperatures are chosen to satisfy the equilibrium condition of constant pressure from $\mathbf{B}_0 \cdot \nabla(n_0 T_{e0,i0}) = 0$, using $T_{e0}^{eq} = 100 \text{ eV}$ and $T_{i0}^{eq} = 200 \text{ eV}$ at the equator. The time-dependent

plasma response is adiabatic with a constant ratio T_i/T_e along the field line.

5.1. Dipolar FLRs

[18] Using the ambient plasma conditions described above, the first case considered corresponds to a small negative value of δ (as computed in the envelope approximation) [Rankin *et al.*, 1999]: $\delta = -5.04 \times 10^{-6} R_e^2$. For the assumed simulation parameters, the SAW period for the driven L shell 7 is approximately 1.1 min. To excite a SAW, we impose the same external monochromatic perturbation of the scalar potential ϕ as in our Box model. In this case, the frequency of the external driver is determined by the length of the resonant field line from one ionosphere to another and by the equilibrium Alfvén velocity profile along the field line. The external driver in the right-hand side of equation (1) causes the wave to grow and propagate to the ionosphere. Since the frequency ω of the driver matches the

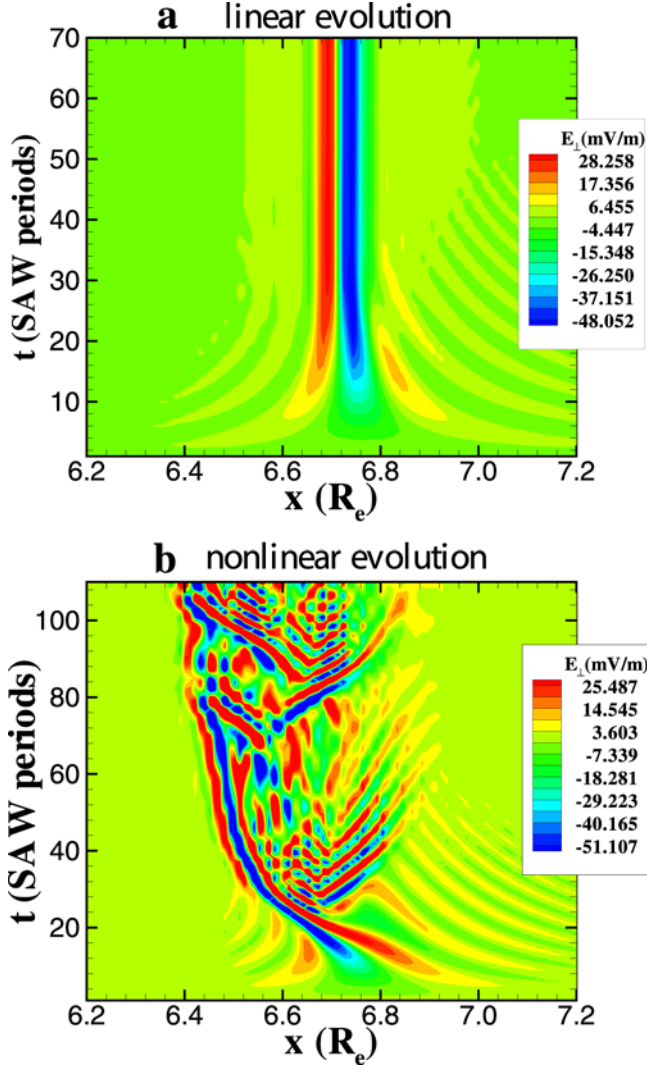


Figure 5. Dynamic evolution of electric field component perpendicular to the magnetic field E_{\perp} at the EP in a dipolar model: (a) linear case and (b) nonlinear case.

frequency of the fundamental SAW mode along the field line at $L = 7$, standing SAWs are formed due to reflection from the perfectly conducting ionospheres.

[19] The imposed driver causes the SAW to narrow and grow linearly in time. This initial phase of FLR evolution corresponds to linear phase mixing and can be explained as follows: Each field line has its own eigenfrequency which, except for the resonant field line, does not coincide exactly with that of the driver. As the wave amplitude grows, the phase difference between the oscillations on nearby field lines increases. This, in turn, produces a modulation of the field structure in the direction perpendicular to the magnetic field, with a scale length that decreases with time. The corresponding wave vector k_{\perp} increases linearly with time, enhancing the wave dispersion that ultimately causes wave propagation in the perpendicular direction. The direction of the propagation depends on the sign of the dispersion coefficient, as discussed earlier. The various stages of this process are illustrated in Figure 5a, which shows a representative evolution of FLRs in the equatorial plane in the linear approximation. We note that the equilibrium

parameters used in this simulation yield a very small value for the dispersion coefficient. As a consequence, there is very little perpendicular propagation of the SAW in the linear case.

[20] As noted in the box model, the linear approximation with small dispersion leads to a static standing wave structure in which dispersive effects are too small to make significant contributions to wave energy propagation. On the other hand, the full nonlinear solutions predict a significant Earthward displacement of the resonance position and a much broader and more intricate wave structure. In particular, the time-dependent nonlinear spatial structuring illustrated in Figure 5b results in part from an acceleration of the timescale for dispersion. To understand this, we refer to equation (8) and note that the timescale for dispersive effects and the corresponding spatial scale is determined by the Alfvén velocity gradient l_{ω} . This gradient is significantly steepened by density fluctuations on the resonant field line, and it is the triggering of small-scale dispersive waves by this effect and their nonlinear interaction with ion acoustic waves that leads to the complicated spatiotemporal structure evident in Figure 5b. Note that the amplitude of the perpendicular electric field is much larger than in the box model.

[21] Figure 6 shows the temporal evolution and radial dependence of the perpendicular electric field and parallel current at the EP Figures 6a–6b and an altitude of $1.2 R_e$ (Figures 6c–6f) for $t = 23$ and 46 SAW periods, respectively. The dotted lines in Figure 6 correspond to the relative density perturbation at the corresponding magnetospheric location. At an altitude of $1.2 R_e$, the density fluctuations remain relatively small (under 8%), and the perturbed fields have properties similar to those obtained in the linear approximation up to 23 periods (Figures 6a, 6c, and 6e), although the spatial scale is significantly compressed in the perpendicular direction. At later times (Figures 6b, 6d, and 6f), the density perturbation increases (above 10%), and the nonlinear spatiotemporal structuring of the wave fields becomes apparent. This aspect of the dynamics of coupled SAWs and IAWs may conveniently be referred to as nonlinear phase mixing, as discussed by Lu *et al.* [2003]. There is a density accumulation at the EP, Figures 6a–6b, and a density depletion near the ionosphere, Figures 6c–6f, both of which act to trap the FLR wave fields. The maximum density accumulation, Figure 6a with $\delta\rho/\rho_0 = 1.7$, and density depletion, Figures 6d and 6f with $\delta\rho/\rho_0 = -0.16$, are not on the driven $L = 7$ magnetic shell but are closer to the Earth (on the shell $L \sim 6.5$ – 6.7). The resonance position also moves Earthward, from $L = 7$ to $L = 6.7$ at $t = 23$ SAW periods, due to dispersion and nonlinearity. Across the resonance, E_{\perp} and j_{\parallel} both have a 180° phase shift, and their maximum amplitudes are of the order of 100 mV/m and $30 \mu\text{A}/\text{m}^2$, respectively, which is in the range of observations of FLRs.

[22] As discussed above, one significant characteristic of Figure 6 is that the FLR is trapped inside density perturbations driven by SAW ponderomotive forces. There are two turning points on either side of the resonance, which can be more clearly seen from Figures 6d and 6f. The nonlinear steepening of the perpendicular profile of the Alfvén velocity by the ponderomotive force changes the frequency of SAW oscillations, and this nonlinear frequency shift increases in proportion to the magnitude of density pertur-

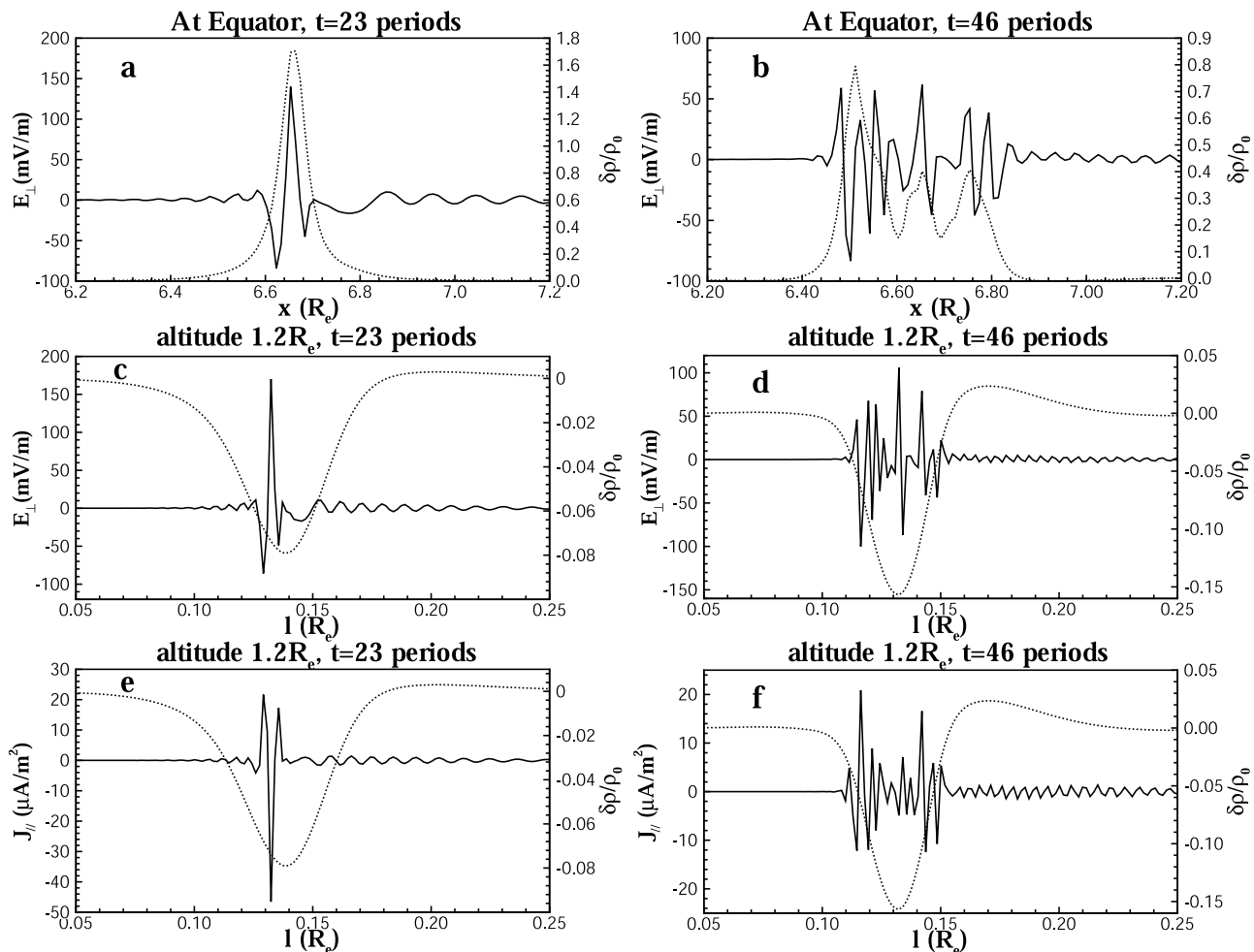


Figure 6. Radial dependence of perpendicular electric field E_{\perp} and parallel current j_{\parallel} at the equator and an altitude $1.2 R_e$ for $t = 23$ and 46 periods, respectively. The dotted line is the relative density perturbation. l corresponds to the distance in R_e from the inner boundary.

bations. Correspondingly, k_{\perp} increases with time much faster than it would due to linear phase mixing alone. Profile steepening (generation of IAWs) results in nonlinear phase mixing that terminates at a level where dispersive effects come into play. At this stage, dispersive and ion acoustic waves appear and propagate away from the resonant field line, the former being reflected from the turning points as discussed above. The temporal aspects of the interplay between density perturbations (IAWs) and dispersive effects has been examined in more detail by *Lu et al.* [2003]. The competition between the dispersive and nonlinear effects is particularly important in the regions where the wave amplitude is high and the dispersion is small. The dispersive effects also modify the eigenfrequency of the FLR, and a corresponding linear mechanism leading to the decoupling of SAWs from the driver was discussed by *Streltsov* [1999].

[23] The time-dependent nonlinear substructuring of wave fields in our model offers one possible explanation for certain features of long-period auroral arcs [e.g., *Samson et al.*, 1991; *Samson et al.*, 1996], which are typically highly localized in latitude. This characteristic feature is common to all our results, which exhibit complicated wave dynamical processes within latitudinally narrow density perturbations. This is illustrated in Figures 7a and 7b, which shows the two-

dimensional spatial distribution of the relative density perturbation, $\delta\rho/\rho_0$, at two representative times during the evolution of FLRs. We note again that FLR wave fields expel plasma from the ionospheric ends of the field line, forming the observed density cavity, negative $\delta\rho/\rho_0$ in white in Figures 7a and 7b. The expelled plasma moves from high latitudes toward the equator (along field lines) where it accumulates, positive $\delta\rho/\rho_0$ is in black in Figures 7a and 7b. It can be seen that the width of the density structure narrows with time and its depth (accumulation) increases.

[24] The net effect of density fluctuations on a given field line is that it causes the SAW eigenfrequency to decrease. Eventually, SAWs excited on a given field line decouple from the driver, leading to instantaneous and local nonlinear wave saturation (nonlinear phase mixing). Figure 7c shows the profile of the maximum (in the perpendicular direction) $\delta\rho/\rho_0$ along the magnetic field line for shell $L = 6.7$ at $t = 23$ SAW periods. For the shell $L = 6.7$, the maximum accumulation occurs at the equator with $\delta\rho/\rho_0 = 0.5$, and the minimum density is not located at the ionospheric boundaries but in the altitude range $2-4 R_e$, with its maximum depletion $\delta\rho/\rho_0 = -0.21$ at $3 R_e$ altitude, at $t = 23$ SAW periods. Unlike *Rankin et al.* [1999], in which the density accumulates at a rate that is much slower than the depletion

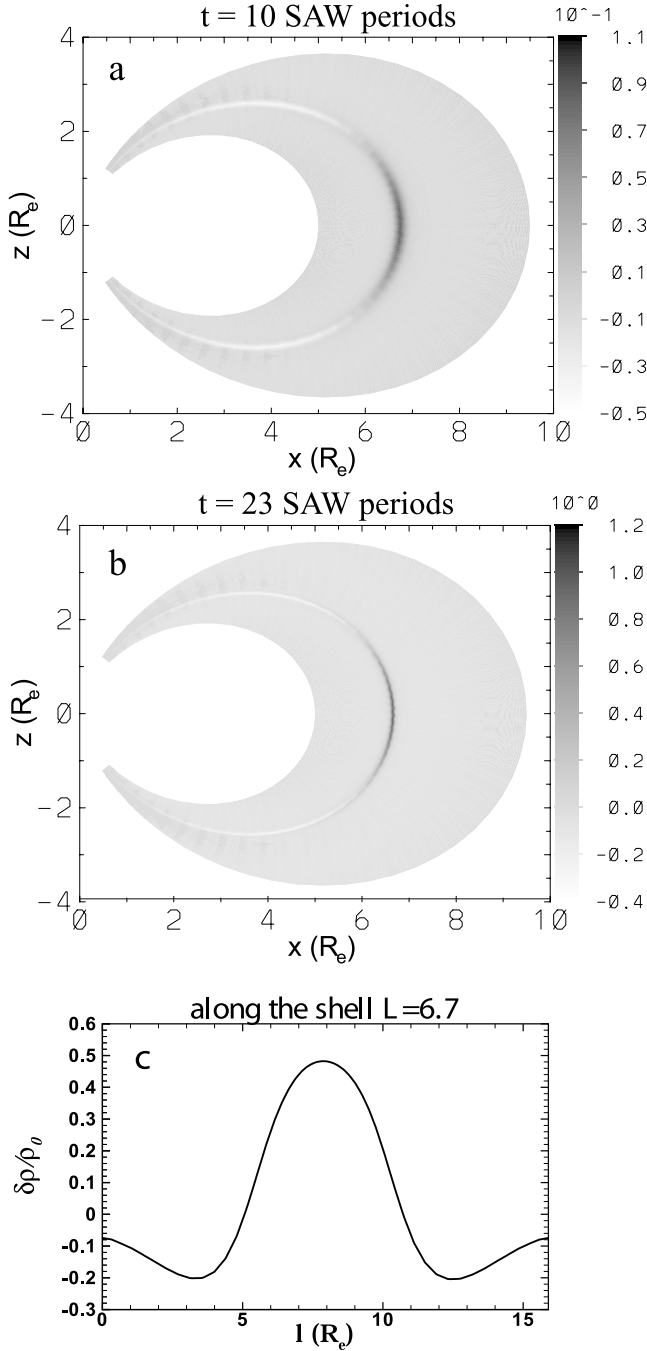


Figure 7. Spatial distribution of the relative density $\delta\rho/\rho_0$. Figures 7a and 7b are two-dimensional distributions of $\delta\rho/\rho_0$ at $t = 10$ and 23 SAW periods, respectively; Figure 7c is the $\delta\rho/\rho_0$ along the shell $L = 6.7$ at $t = 23$ SAW periods. l corresponds to the distance in R_e from the bottom boundary.

rate, here the density accumulates at a rate that is faster than the depletion, since the accumulation region extends over a much narrower region (see Figures 7a and 7b). The ionospheric density cavity may result in an enhancement of auroral electric fields [Streltsov *et al.*, 1998; Tikhonchuk and Rankin, 2000; Song and Lysak, 2001].

[25] It is worth noting that the large density perturbations observed in our simulations clearly indicate the necessity to go beyond the use of linear and/or envelope approaches to

the study of FLRs. We note also that the notion of an auroral plasma cavity has been introduced by Benson and Calvert [1979] and Calvert [1981], on the basis of ISIS-1 and Hawkeye data. Mid-altitude in situ measurements within auroral plasma cavities have also been made by DE-1 [Persoon *et al.*, 1981]. At these altitudes, the cavities are characterized by very low plasma density, and the minimum density frequently reaches values below 0.3 per cm^3 in the altitude range 2–4.6 R_e . Freja also observed density decreases by more than two orders of magnitude (from 1000 to 10 particles per cm^3) at about 1700 km altitude [Lundin *et al.*, 1994]. The FLR model discussed here successfully explains the formation of density cavities and may point to a common process (ponderomotive forces) for density cavity formation that is consistent with many observations. The PF mechanism is also consistent with outflowing ions that have been observed in association with auroral potential structures.

5.2. FLRs in Stretched Magnetic Field Lines

[26] The reported FLR frequency at the midnight sector is 1–4 mHz at auroral latitudes [e.g., Samson *et al.*, 1991]. Generally, FLR frequencies calculated for the dipolar magnetosphere are one order of magnitude larger than those observed. Especially during weakly active magnetospheric conditions, field lines are more stretched in the midnight region, and stretching of Earth’s magnetic field offers a possible explanation for anomalously low frequency SAWs. Rankin *et al.* [2000] and Lui and Cheng [2001] calculated the linear evolution of FLRs in stretched magnetic field lines and obtained frequencies that are consistent with observations. However, they limited their analysis to the linear case, without inclusion of dispersive effects.

[27] In order to illustrate the effect of nonlinear and dispersive effects in the dynamic evolution of FLRs in a stretched magnetic field topology, we consider a typical stretched case with the same background conditions as in the dipolar case discussed above. We assume that the magnetosphere is axially symmetric and that magnetic field lines in the meridional z, x plane are approximated by the T96 model [Tsyganenko, 1996] for a solar wind pressure of 1.0 nPa, with $Dst = -10$ nT, $B_y = 0$, and $B_z = -1$ nT. Correspondingly, the intercept of the dipolar shell $L = 6.5$ is stretched to 9 R_e at the EP. The calculated FLR eigenmode frequency for this stretched L -shell is 4.0 mHz, which is in agreement with the upper range of observed values. This set of parameters provides an illustrative example of the types of geometry that can be simulated with our code and as an example of the effect of stretching on FLRs.

[28] Figure 8 shows the time-dependent nonlinear spatial structuring of the dispersive FLR in the equatorial plane. Compared with the dipolar case of Figure 5b, one obvious feature of Figure 8 is the anti-Earthward propagating waves at earlier times, implying that much stronger dispersive effects are observed. The background parameters correspond to a relatively large and positive value of $\delta = 6.0 \times 10^{-5} R_e^2$ on the initially resonant field line. In this case, thermal effects dominate, resulting in anti-Earthward propagating waves. Note that in the EP, E_{\perp} is significantly smaller than in the dipolar case. In a stretched topology, nonlinearity again causes the resonance to move Earthward until it reaches a location where the time-dependent dispersion becomes very

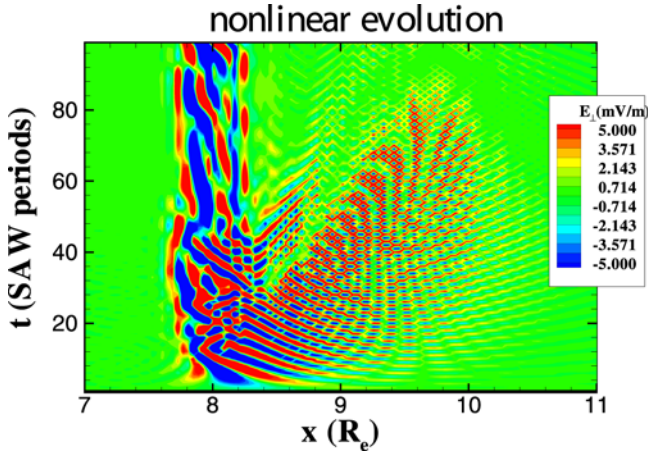


Figure 8. Dynamic evolution of electric field component perpendicular to the magnetic field E_{\perp} at the EP in a sampled stretched model for a nonlinear FLR.

small. At this stage, the FLR undergoes similar dynamics to the dipolar cases discussed above, which also correspond to small dispersion. For example, in Figure 8, the FLR is eventually trapped around $7.7 R_e$, where the background dispersive parameter $\delta = -1.0 \times 10^{-5} R_e^2$. Figure 9 shows the radial dependence of the background dispersive parameter δ (computed using the envelope model), indicating that it changes sign in the vicinity of the region where the FLR becomes localized within a narrow region.

[29] As in the dipolar case, the trapped SAWs that emerge in a stretched topology are confined to latitudinally narrow density perturbations. Figure 10 shows the 2-D spatial density perturbation, $\delta\rho/\rho_0$ at three different times. Initially, Figure 10a, the dynamics is similar to the dipolar case. However, because of the relatively large dispersion, density structures propagate anti-Earthward of the resonance, Figure 10b. These structures trap FLR wave energy within them, but they are eventually removed by nonresonant phase mixing, Figure 10c. This can also be seen in Figure 8, where the wave structure propagating anti-Earthward of $9 R_e$ eventually dissipates. Figure 11 shows the radial dependence of E_{\perp} and J_{\parallel} at the EP and an altitude $1.2 R_e$ for 23, 46, and 80 periods, respectively. At $t = 23$ and 46 periods, the waves propagate anti-Earthward. When the time-dependent disper-

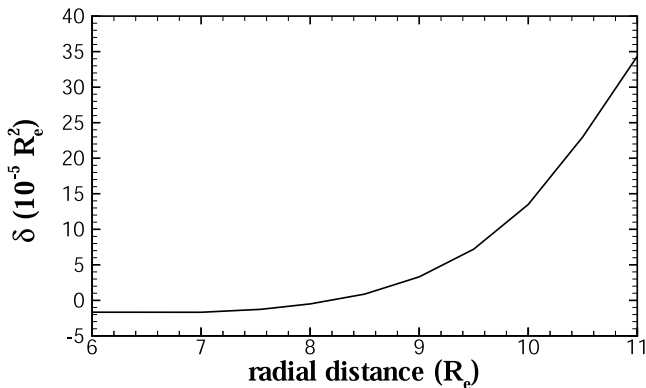


Figure 9. Radial dependence of dispersive parameter δ in the sampled stretched case.

sion becomes very small, the perpendicular density profile and the FLR wave fields more efficiently steepen, resulting in nonlinear phase mixing and the localization and complicated structure of the FLR that was discussed in the dipolar case. Finally, the SAW is trapped inside nonlinear density perturbations; for example at $t = 80$ periods of Figure 11. This result is important because it offers a potential explanation as to why FLRs with certain frequencies map to specific latitudes. It is also confirmed from Figures 11 and 6 that the stretched geometry results in a larger current and a smaller perpendicular electric field.

6. Summary and Discussion

[30] A new finite element code, TOPO, is used to investigate the nonlinear interaction of dispersive field line resonances and ion acoustic waves (IAWs). Initially, a Cartesian box model is considered to demonstrate the reliability of our numerical solution in describing linear FLR evolution. Then the effects of electron inertia, ion Larmor radius correction, and electron thermal pressure are investigated in the nonlinear evolution of FLRs in dipolar

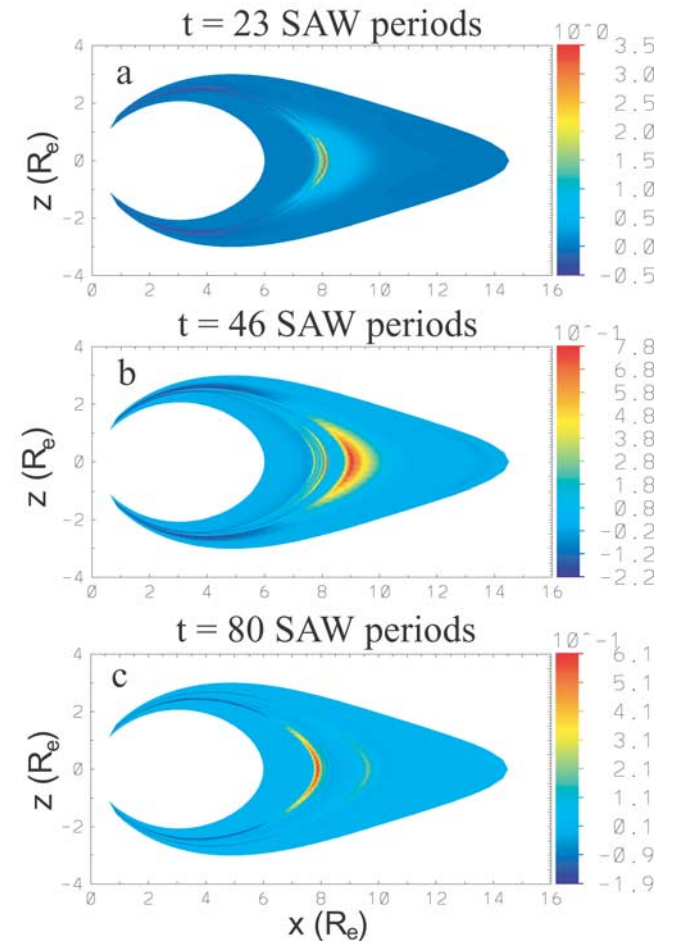


Figure 10. Meridional distribution of density perturbation $\delta\rho/\rho_0$ in sampled, stretched magnetic field lines defined by the T96 model. The chosen solar wind condition corresponds to the dipolar shell $L = 6.5$ stretched to $9 R_e$ at the equator. The $L = 6.5$ field line eigenfrequency is consistent with observations.

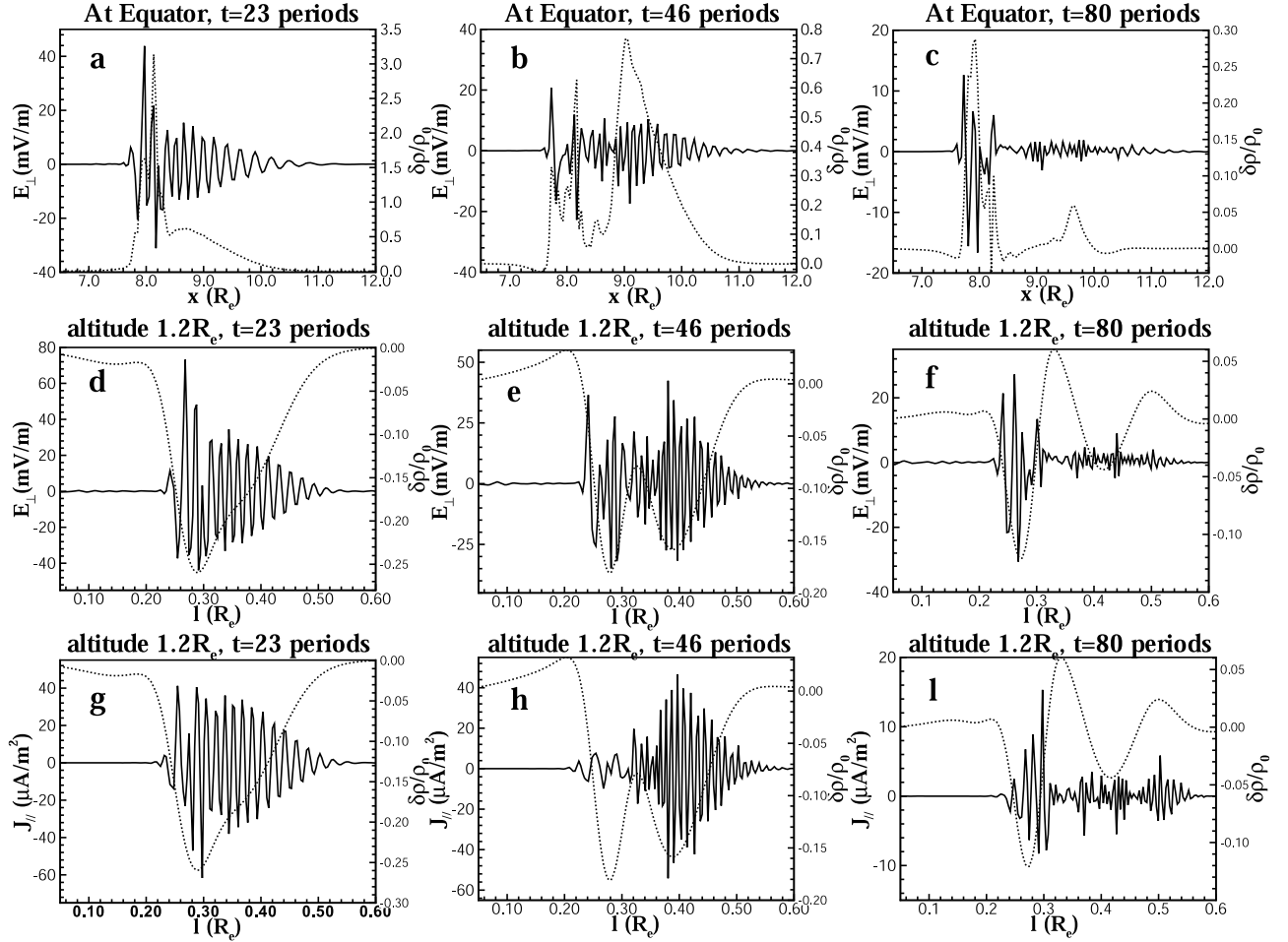


Figure 11. Radial dependence of perpendicular electric field E_{\perp} and parallel current j_{\parallel} at the equator and an altitude $1.2 R_e$ for $t = 23, 46,$ and 80 periods in the sampled stretched case, respectively. The dotted line is the relative density perturbation. l corresponds to the distance in R_e from the inner boundary.

and stretched magnetic fields. A detailed discussion of the characteristics of density fluctuations, field-aligned currents, and magnetic and electric fields has been presented.

[31] Our work differs from *Frycz et al.* [1998] and *Rankin et al.* [1999] mainly in that we treat the full nonlinear self-consistent set of reduced MHD equations, as opposed to the linearized envelope model. We show that for realistic magnetospheric conditions, the envelope model breaks down and new nonlinear behavior results. Time-dependent dispersion and density steepening lead to a rapid acceleration of the timescale for phase mixing to small spatial scales and a strong interaction between wave dispersion and nonlinearity results. Consequently, shear Alfvén waves become trapped between turning points inside latitudinally localized nonlinear density perturbations. This results in spatiotemporal nonlinear structuring of FLRs that is associated with an overlap of timescales for dispersion and nonlinearity. In particular, ponderomotive forces change the dispersive scale, accelerating the appearance of dispersive waves which strongly interact with IAWs.

[32] Similar nonlinear dynamics results in stretched topologies, and in particular, field line stretching and ponderomotive density redistribution lead to a significant reduction in FLR eigenfrequencies, bringing them into the range of

observations. In stretched topologies, stronger dispersive effects are present initially, but nonlinearity and electron inertia act to move the FLR to a location where dispersion is small. Finally, shear Alfvén wave becomes trapped inside nonlinear density perturbations at latitudinal field line locations where the ambient wave dispersion changes sign. This important conclusion offers a potential explanation as to why FLRs with certain frequencies map to specific latitudes. Our model predicts density perturbations that can be comparable to the equilibrium background density. Our results are also consistent, in a qualitative sense, with observational features of discrete auroral arcs and provide an important insight into the dynamics of SAWs and auroral activity.

[33] It should be mentioned that this calculation is limited to low- β plasma. If the ion temperature is high enough, i.e., $(k_{\perp} \rho_i)^2 > 1$, the 3/4 ion Larmor gyroradius correction in equation (1) will be invalid and the Padé's approximation should be used [*Johnson and Cheng*, 1997; *Streltsov et al.*, 1998]. High temperature will increase the wave dispersion and so may cause different perpendicular dynamics of FLRs. For high- β plasma, fast mode has to be considered.

[34] In future work, we will present a more detailed discussion of the dynamics of FLRs in stretched magnetic field lines. In particular, we will more fully assess the role

played by different drivers for FLRs, as in this study we have only considered a monochromatic driver. Finally, we note that although the IAWs excited in our model are driven, the effect of Landau damping of these waves needs to be more fully assessed.

[35] **Acknowledgments.** This work was supported in part by the Canadian Space Agency and the Natural Sciences and Engineering Research Council of Canada. Our work made use of the infrastructure and resources of Multimedia Advanced Computational Infrastructure, funded in part by the Canada Foundation for Innovation, Alberta Innovation and Science Research Investment Program, and the Universities of Alberta and Calgary.

[36] Lou-Chuang Lee thanks Anatoly V. Sreltsov for the assistance in evaluating this paper.

References

- Benson, R. F., and W. Calvert, ISIS 1 observations of the source of auroral kilometric radiation, *Geophys. Res. Lett.*, **6**, 479, 1979.
- Bhattacharjee, A., C. A. Kletzing, Z. W. Ma, C. S. Ng, N. F. Otani, and X. Wang, Four-field model for dispersive field-line resonances: Effects of coupling between shear-Alfvén and slow modes, *Geophys. Res. Lett.*, **26**, 3281, 1999.
- Boehm, K. H., C. W. Carlson, J. P. McFadden, J. H. Clemmons, and F. S. Mozer, High-resolution sounding rocket observations of large-amplitude Alfvén waves, *J. Geophys. Res.*, **95**, 12,157, 1990.
- Calvert, W., The auroral plasma cavity, *Geophys. Res. Lett.*, **8**, 919, 922, 1981.
- Chen, L., and A. Hasegawa, A theory of long period magnetic pulsations: 1. Steady state excitation of field line resonance, *J. Geophys. Res.*, **79**, 1024, 1974.
- Cheng, C. Z., T. C. Chang, C. A. Lin, and W. H. Tsai, Magnetohydrodynamic theory of field line resonances in magnetosphere, *J. Geophys. Res.*, **98**, 11,339, 1993.
- Cummings, W. D., R. J. O'Sullivan, and P. J. Coleman Jr., Standing Alfvén waves in the magnetosphere, *J. Geophys. Res.*, **74**, 778, 1969.
- Frycz, P., R. Rankin, J. C. Samson, and V. T. Tikhonchuk, Nonlinear field line resonances: Dispersive effects, *Phys. Plasmas*, **5**, 3565, 1998.
- Goertz, C. K., Kinetic Alfvén waves on auroral field lines, *Planet. Space Sci.*, **32**, 1387, 1984.
- Hasegawa, A., Particle acceleration by MHD surface wave and formation of aurora, *J. Geophys. Res.*, **81**, 5083, 1976.
- Hasegawa, A., and M. M. Wakatani, Finite-larmor-radius magnetohydrodynamic equations for microturbulence, *Phys. Fluids*, **26**, 2770, 1983.
- Johnson, J. R., and C. Z. Cheng, Kinetic Alfvén waves and plasma transport at the magnetopause, *Geophys. Res. Lett.*, **24**, 1423, 1997.
- Kadomtsev, B. B., and O. P. Pogutse, Nonlinear helical perturbations of a plasma in the tokamak, *Sov. Phys. JETP*, **38**, 283, 1974.
- Leonovich, A. S., and V. A. Mazur, A model equation for monochromatic standing Alfvén waves in the axially symmetric magnetosphere, *J. Geophys. Res.*, **102**, 11,443, 1997.
- Lu, J. Y., R. Rankin, R. Marchand, and V. T. Tikhonchuk, Nonlinear acceleration of dispersive effects in field line resonances, *Geophys. Res. Lett.*, **30**(10), 1540, doi:10.1029/2003GL016929, 2003.
- Lui, A. T. Y., and C. Z. Cheng, Resonance frequency of stretched magnetic field lines based on a self-consistent equilibrium magnetosphere model, *J. Geophys. Res.*, **106**, 25,793, 2001.
- Lundin, R., L. Eliasson, G. Haerendel, M. Boehm, and B. Holback, Large scale auroral density cavities observed by Freja, *Geophys. Res. Lett.*, **21**, 1903, 1994.
- Lysak, R. L., and Y. Song, Kinetic theory of the Alfvén wave acceleration of auroral electrons, *J. Geophys. Res.*, **108**(A4), 8005, doi:10.1029/2002JA009406, 2003.
- Marchand, R., and M. Shoucri, Numerical simulation of the excitation and evolution of high azimuthal mode number coherent vortices in hollow magnetized electron columns, *J. Plasma Phys.*, **65**, 151, 2001.
- Marchand, R., and M. Simard, Finite element modelling of Tdev edge and divertor with $\mathbf{E} \times \mathbf{B}$ drifts, *Nucl. Fusion*, **37**, 1629, 1997.
- Persoon, A. M., D. A. Gurnett, W. K. Peterson, J. H. Waite Jr., J. L. Burch, and J. L. Green, Electron density depletions in the nightside auroral zone, *J. Geophys. Res.*, **93**, 1871, 1988.
- Rankin, R., F. Fenrich, and V. T. Tikhonchuk, Shear Alfvén waves on stretched magnetic field lines near midnight in Earth's magnetosphere, *Geophys. Res. Lett.*, **27**, 3265, 2000.
- Rankin, R., P. Frycz, V. T. Tikhonchuk, and J. C. Samson, Ponderomotive saturation of magnetospheric field line resonances, *Geophys. Res. Lett.*, **22**, 1741, 1995.
- Rankin, R., J. C. Samson, and P. Frycz, Simulation of driven field line resonances in the Earth's magnetosphere, *J. Geophys. Res.*, **98**, 21,341, 1993.
- Rankin, R., J. C. Samson, V. T. Tikhonchuk, and I. Voronkov, Auroral density fluctuations on dispersive field line resonances, *J. Geophys. Res.*, **104**, 4399, 1999.
- Rankin, R., and V. T. Tikhonchuk, Numerical simulations and simplified models of nonlinear electron inertial Alfvén waves, *J. Geophys. Res.*, **103**, 20,419, 1998.
- Ruohoniemi, J. M., R. A. Greenwald, K. B. Baker, and J. C. Samson, HF radar observations of Pc 5 field resonances in a midnight/early morning MLT sector, *J. Geophys. Res.*, **96**, 15,697, 1991.
- Samson, J. C., D. D. Wallis, T. J. Hughes, F. Creutzberg, J. M. Ruohoniemi, and R. A. Greenwald, Substorm intensifications and field line resonances in the nightside magnetosphere, *J. Geophys. Res.*, **97**, 8495, 1992.
- Samson, J. C., T. J. Hughes, F. Creutzberg, D. D. Wallis, R. A. Greenwald, and J. M. Ruohoniemi, Observations of detached, discrete arc in association with field line resonances, *J. Geophys. Res.*, **96**, 15,683, 1991.
- Samson, J. C., L. L. Cogger, and Q. Pao, Observations of field line resonances, auroral arcs, an auroral vortex structures, *J. Geophys. Res.*, **101**, 17,373, 1996.
- Samson, J. C., and R. Rankin, The coupling of solar wind energy to MHD cavity modes, waveguide modes, and field line resonances in the Earth's magnetosphere, in *Solar Wind Sources of Magnetospheric Ultra-Low Frequency Waves*, *Geophys. Monogr. Ser.*, vol. 81, edited by M. Engebretson, K. Takahashi, and M. Scholer, pp. 253, AGU, Washington, D. C., 1994.
- Song, Y., and R. L. Lysak, The physics in the auroral dynamo regions and auroral particle acceleration, *Phys. Chem. Earth*, **26**, 33, 2001.
- Southwood, D. J., Some features of field line resonances in the magnetosphere, *Planet. Space Sci.*, **22**, 483, 1974.
- Southwood, D. J., and M. G. Kivelson, The effects of parallel inhomogeneity on magnetospheric hydromagnetic wave coupling, *J. Geophys. Res.*, **91**, 6871, 1986.
- Strauss, H. R., Nonlinear three-dimensional magnetohydrodynamics of noncircular tokamaks, *Phys. Fluids*, **19**, 134, 1976.
- Stasiewicz, K., G. Gustafsson, G. Marklund, P.-A. Lindqvist, J. Clemmons, and L. Zanetti, Cavity resonators and Alfvén resonance cones observed on Freja, *J. Geophys. Res.*, **102**, 2565, 1997.
- Streltsov, A. V., Dispersive width of the Alfvén field line resonance, *J. Geophys. Res.*, **104**, 22,657, 1999.
- Streltsov, A. V., and W. Lotko, Dispersive field line resonances on auroral field lines, *J. Geophys. Res.*, **100**, 19,457, 1995.
- Streltsov, A. V., and W. Lotko, Dispersive, nonradiative field line resonances in a dipole magnetic field geometry, *J. Geophys. Res.*, **102**, 27,121, 1997.
- Streltsov, A. V., and W. Lotko, Dispersive, Small-scale, "electrostatic" auroral structures and Alfvén waves, *J. Geophys. Res.*, **104**, 4411, 1999.
- Streltsov, A. V., W. Lotko, J. R. Johnson, and C. Z. Cheng, Small-scale, dispersive field line resonances in the hot magnetospheric plasma, *J. Geophys. Res.*, **103**, 26,559, 1998.
- Tikhonchuk, V. T., and R. Rankin, Electron kinetic effects in standing shear Alfvén waves in the dipolar magnetosphere, *Phys. Plasma*, **7**, 2630, 2000.
- Tikhonchuk, V. T., and R. Rankin, Parallel potential driven by a kinetic Alfvén wave on geomagnetic field lines, *J. Geophys. Res.*, **107**(A7), 1104, doi:10.1029/2001JA000231, 2002.
- Trondsen, T. S., L. L. Cogger, and J. C. Samson, Observations of asymmetric, multiple auroral arcs, *Geophys. Res. Lett.*, **24**, 2945, 1997.
- Tsyganenko, N. A., Effects of the solar wind conditions on the global magnetospheric configuration as deduced from databased models, in *Proc. of Third Int. Conf. on Substorms ICS-3, ESA SP-389*, pp. 181, Eur. Space Agency, Paris, 1996.
- Walker, A. D. M., J. M. Ruohoniemi, K. B. Baker, R. A. Greenwald, and J. C. Samson, Spatial and temporal behavior of ULF pulsations observed by the Goose Bay HF radar, *J. Geophys. Res.*, **97**, 12,187, 1992.
- Wei, C. Q., J. C. Samson, R. Rankin, and P. Frycz, Electron inertial effects on geomagnetic field line resonances, *J. Geophys. Res.*, **99**, 11,265, 1994.

J. Y. Lu, R. Marchand, and R. Rankin, Department of Physics, University of Alberta, Edmonton, Alberta, Canada T6G 2J1. (jlu@space.ualberta.ca)
 V. T. Tikhonchuk, Centre Laser Intenses et Applications, Université Bordeaux 1, 351 Cours de la Liberation, 33405 Talence cedex, France. (tikhon@celia.u-bordeaux.fr)

J. Wanliss, Embry-Riddle Aeronautical University, 600 S. Clyde Morris Blvd., Daytona Beach, FL 32114, USA. (james.wanliss@erau.edu)